Rock and Soil Mechanics

Volume 42 | Issue 8 Article 2

12-16-2021

Research on the mechanical characteristics of granite failure process under true triaxial stress path

Jie LIU
School of Science, Qingdao University of Technology, Qingdao, Shandong 266033, China

Li-ming ZHANG
Cooperative Innovation Center of Engineering Construction and Safety in Shandong Blue Economic Zone, Qingdao University of Technology, Qingdao, Shandong 266033, China, dryad_274@163.com

Yu CONG
Cooperative Innovation Center of Engineering Construction and Safety in Shandong Blue Economic Zone, Qingdao University of Technology, Qingdao, Shandong 266033, China

Zai-quan WANG
Cooperative Innovation Center of Engineering Construction and Safety in Shandong Blue Economic Zone, Qingdao University of Technology, Qingdao, Shandong 266033, China

Custom Citation

LIU Jie, ZHANG Li-ming, CONG Yu, WANG Zai-quan, . Research on the mechanical characteristics of granite failure process under true triaxial stress path[J]. Rock and Soil Mechanics, 2021, 42(8): 2069-2077.

Rock and Soil Mechanics 2021 42(8): 2069−2077 ISSN 1000−7598
https: //doi.org/10.16285/j.rsm.2021.5110 rocksoilmech.researchcommons.org/journal

Research on the mechanical characteristics of granite failure process under true triaxial stress path

LIU Jie[1], ZHANG Li-ming[1, 2], CONG Yu[1, 2], WANG Zai-quan[1, 2]

1. School of Science, Qingdao University of Technology, Qingdao, Shandong 266033, China

2. Cooperative Innovation Center of Engineering Construction and Safety in Shandong Blue Economic Zone, Qingdao University of Technology, Qingdao, Shandong 266033, China

Abstract: The true triaxial loading and unloading tests on granite were conducted to obtain the mechanical characteristics of the granite in the construction area of an underground cavern. The stability of the surrounding rock, the characteristic stress, the failure mode and the brittleness characteristics were mainly analyzed in this work. In addition, the evolution laws of total energy and dissipated energy with axial strain were explored. Results show that under the true triaxial loading and unloading stress paths, the failure modes of granite are both tensile and shear composite failure, and characteristics of high damage stress and brittleness are obviously observed. A new brittleness index is proposed to evaluate rock brittleness by using volumetric strain curve. It is found that the brittleness of granite is higher under unloading conditions. In the true triaxial loading test, the change trend of total energy with axial strain goes through three stages: slow increase, rapid increase, and steady increase. In the true triaxial unloading test, the dissipated energy increases rapidly at the moment of unloading, and its proportion in the energy distribution exceeds the elastic strain energy, which becomes the main energy consumption. The energy dissipation value of the granite sample in the loading test is obviously greater than that in the unloading test. It indicates that more energy is required for samples under the loading path to produce damage, which is safer than the unloading path. The particle flow PFC^{3D} is used to simulate the true triaxial loading and unloading test of granite in this study. The failure mode and the crack distribution of the numerical simulation results are basically consistent with results of the laboratory test. Then the numerical model is used to simulate the rapid unloading failure process of granite. It is found that the rock sample particle ejection damage will occur at the end of the model, similar to a rock burst.

Keywords: true triaxial test; mechanical properties; energy evolution

1 Introduction

The excavation and unloading in underground engineering change the initial stress of rock mass, e.g., the unloading in the biaxial directions or one direction in surrounding rocks will result in the transition of three-direction confinement of the rock to one-direction or two-direction confinement. The unloading in highly confined surrounding rocks induces seriously disasters such as rock burst, collapse, and roof fall[1−2], which threaten the safety and stability of neighboring engineering structures. Therefore, it is of great significance to understand the mechanical properties of the rock mass subjected to true triaxial stress loading paths.

Many researches on the laboratory test were conducted to understand the mechanical behaviours of rock failure under true triaxial loading and unloading conditions, as well as the change in *in-situ* stress after the excavation. For example, He et al.[3] simulated the process of rockburst after a rapid unloading of stress in one direction in true triaxial test, and found that the failure modes of rockburst can be divided into the tensile failure, the fluctuant cleavage fracture and the overall cleavage fracture. Chen et al.[4] and Feng et al.[5] carried out the true triaxial unloading test for granites, and analyzed the rebound deformation and elastic brittle failure characteristics of granite based on acoustic emission information. Su et al.[6] used the acoustic emission to investigate rockburst under true triaxial loading conditions, and revealed the temporal and spatial evolution characteristics of acoustic emission in rockburst. Moreover, the ratio of the height to width and the intermediate principal stress of the sample were found to have an effect on the failure mode, peak strength and failure degree of the hard rock in the true triaxial unloading test[7]. Rong et al.[8] conducted true triaxial disturbance unloading tests to analyze the deformation and failure characteristics of rocks, and the evolution of mechanical parameters under different stress paths under high confinement were understood. The results from the true triaxial compression test of volcanic rock by Kong et al.[9] indicated that the brittleness of rock failure increases with the increase of the intermediate principal stress. Zhang et al.[10] also found that the Mohr-Coulomb criterion was more beneficial for revealing the strength characteristics of the rock than the Drager-Prager criterion for the initial *in-situ* stress reduction tests under different overburden depths and different stress paths.

Energy accumulation and dissipation are associated with the process of rock deformation. Xie et al.[11−12] analyzed the energy dissipation and damage of sandstone during the uniaxial compression, and the changes of the strain energy and dissipated energy in the rock under different loading rates, and different loading levels

Received: 15 January 2021 Revised: 10 March 2021
This wok was supported by the National Natural Science Foundation of China (47102322) and the Natural Science Foundation in Shandong Province (ZR2020ME099, ZR2020MD111).
First author: LIU Jie, female, born in 1994, MSc student, focusing on rock mechanics and underground engineering. E-mail:jiessie_79@163.com
Corresponding author: ZHANG Li-ming, male, born in 1977, PhD, Professor, focusing on rock mechanics and underground engineering. E-mail: dryad_274@163.com

were obtained. Additionally, the energy evolution law of red sandstones under different loading rates was performed by Zhang et al.[13]. The rockburst tests on granite were conducted[14–15]. The results indicated that the ejection kinetic energy of rockburst accounts for less than 1% of the elastic strain energy accumulated in the pre-peak stage of the rock sample. Moreover, Cong et al.[16] and Zhang et al.[17–19] conducted conventional triaxial loading and unloading tests on marble and the evolution law of the axial energy and total energy of the rock mass with deformation were achieved.

Currently, the researches on the true triaxial failure of rocks are mainly limited to the analysis of the failure characteristics of rocks. The research on the characteristic stress of the full process of the rock deformation under the true triaxial path and the energy evolution during the true triaxial loading and unloading was overlooked. In this study, the true triaxial loading and unloading failure tests of granite were carried out, and the changes in the characteristic stress throughout the deformation process were presented. Moreover, the characteristics of the brittle failure and high damage stress of granite were revealed, and the evolution law of total energy, elastic energy, as well as the dissipated energy during rock deformation under true triaxial path were discussed.

2 Experimental method

2.1 Rock sample preparation

The monzonite granite sample are cored from an underground cavern and the rock mass is featured with a medium-fine-grained structure and a massive texture. The main mineral components in the sample are quartz, orthoclase, plagioclase, and biotite. The fresh rock blocks collected on site are drilled, polished, and sampled with a size of 50 mm×50 mm×100 mm, as shown in Fig.1. The dry density of the granite in this study is 2.62 g/cm^3, the uniaxial compressive strength, the tensile strength, and the Poisson's ratio are 83.47 MPa, 10.06 MPa, and 0.22.

Fig. 1 Rock samples of the test

2.2 True triaxial test

The test is carried out on the true triaxial testing system[20] independently developed by Institute of Rock and Soil Mechanics, Chinese Academy of Sciences, as shown in Fig.2. This system contains a fully rigid mechanical loading system, a servo control and a data acquisition system. The common tests under uniaxial stress paths, conventional triaxial stress paths, true triaxial stress paths, cyclic loading and unloading, and creep tests can be carried out using this testing system. The maximum axial force of the system is 2 500 kN, and the maximum lateral force is 1 000 kN.

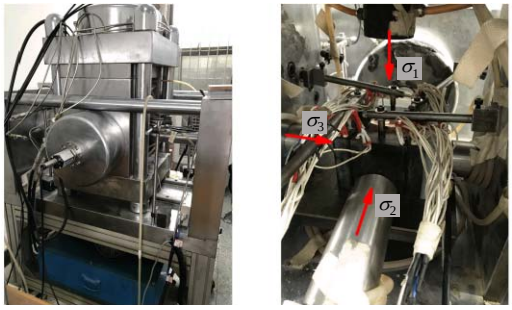

(a) Appearance (b) Internal configuration

Fig. 2 The true triaxial test system

Considering the *in-situ* stresses in the survey report of the sampling site (the maximum horizontal principal stress is 37.9 MPa), the intermediate principal stress and the minimum principal stress of the true triaxial test are set as 40, 30 MPa to reproduce the high *in-situ* stress state of the deep surrounding rock in the laboratory. The stress paths of the true triaxial loading and unloading test are shown in Fig.3 and the specific test processes are as follows:

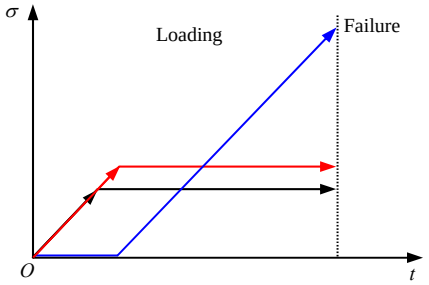

(a) Loading path

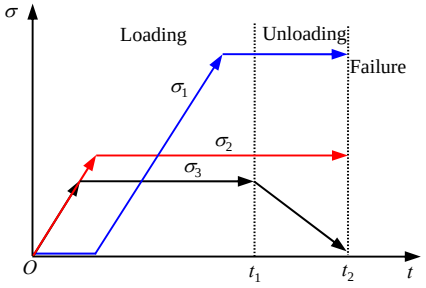

(b) Unloading path

Fig. 3 The test paths used in this study

(1) True triaxial loading test: synchronously increase σ_2 and σ_3 to the set values, and keep σ_2 and σ_3 as constant, load σ_1 at a rate of 0.1 mm/min to the failure of the rock sample, and obtain the peak strength of the rock sample under different confining pressures.

(2) True triaxial unloading test: synchronously increase σ_2 and σ_3 to the set values, keep σ_2 and σ_3 as constant, and load σ_1 at a rate of 0.1 mm/min to 80% stress level of the pre-peak value; maintain the stress in three directions for two minutes, unload σ_3 from one side at different unloading rates (0.3, 0.45, 0.55 mm/min) as shown in Fig.4.

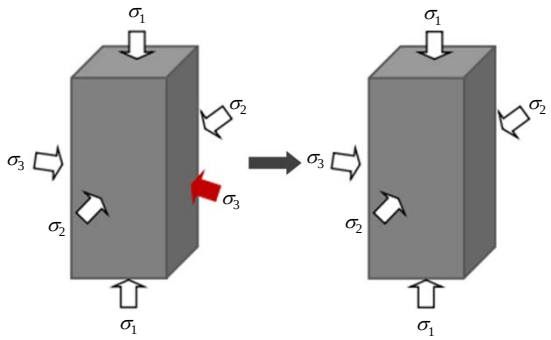

Fig. 4 Schematic diagram of unloading direction

3 Experimental results

3.1 Stress–strain curve and characteristic stress

The stress–strain curve of true triaxial loading tests for granite is shown in Fig.5. The stress–strain curve is divided into four stages using the crack volumetric strain method[16]: the initial compaction stage *OA*, the elastic deformation stage *AB*, the stable crack growth stage *BC* and the unstable crack growth stage *CD*. The granite sample is broken into pieces due to the strong brittle failure in the post-peak stage, which results in quick loss of the bearing capacity of the sample and makes it is difficult to obtain a complete post-peak deformation curve for some samples.

The volumetric strain can be calculated using the following equation

$$\varepsilon_{\mathrm{v}} = \varepsilon_1 + \varepsilon_2 + \varepsilon_3 \tag{1}$$

where ε_1, ε_2 and ε_3 are the principal strains in three directions of the rock sample, respectively; and ε_{v} is the volumetric strain.

The crack volumetric strain is the volume change resulted from the closure and expansion of fractures in rock. The total volumetric strain can be expressed as the sum of the crack volumetric strain and the elastic volumetric strain[21]

$$\varepsilon_{\mathrm{v}}^{\mathrm{c}} = \varepsilon_{\mathrm{v}} - \varepsilon_{\mathrm{v}}^{\mathrm{e}} = \varepsilon_{\mathrm{v}} - \frac{1-2\upsilon}{E}\left(\sigma_1 + \sigma_2 + \sigma_3\right) \tag{2}$$

where σ_1, σ_2 and σ_3 are the principal stresses in three directions of the rock sample, respectively; $\varepsilon_{\mathrm{v}}^{\mathrm{c}}$ and $\varepsilon_{\mathrm{v}}^{\mathrm{e}}$ are the crack volumetric strain and the elastic volumetric strain.

The crack volumetric strain decreases in the compaction stage as shown in Fig.5. The microcrack generated in the elastic stage is not evident and the crack volumetric strain remains constant. In the stable crack growth stage, cracks are formed within the sample, and the curve of the crack volumetric strain decreases. The stress corresponding to this point is regarded as the crack initiation stress σ_{ci}. When the total strain reaches its maximum value, the unstable crack growth stage starts, and this stress is the crack damage stress σ_{cd}. The crack volumetric strain continues to increase, and the rock sample enters the post-peak failure stage after the stress exceeds its maximum.

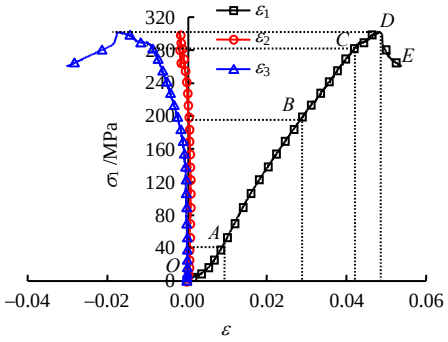

(a) Stress-strain curves

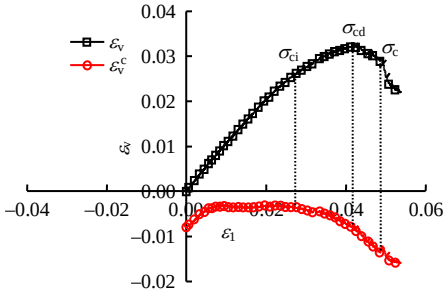

(b) Crack volumetric strain

Fig. 5 Crack volumetric strain and characteristic stress in true triaxial loading tests

The characteristic stresses of granite in true triaxial loading tests calculated by Eqs.(1) and (2) are illustrated in Table 1. The dispersion of parameters and characteristic stresses of sample I-3 is the largest and resulted from the initial cracks in the sample. Therefore, only the results of samples I-1 and I-2 are accounted for computing the average value, and the initiation stress σ_{ci}, damage stress σ_{cd}, and peak stress σ_{c} under confining pressures of $\sigma_2 = 40$ MPa, $\sigma_3 = 30$ MPa are 185.8, 273.6, and 299.8 MPa, respectively.

Table 1 Mechanical parameters and characteristic stresses of granite in true triaxial loading tests

Sample No.	Elastic modulus E /GPa	Poisson's ratio ν	Initiation stress σ_{ci} /MPa	Damage stress σ_{cd} /MPa	Peak stress σ_{c} /MPa	Crack initiation stress ratio	Crack damage stress ratio
Ⅰ-1	9.16	0.23	182.6	267.9	297.5	0.614	0.901
Ⅰ-2	7.21	0.21	189.0	279.2	302.1	0.626	0.924
Ⅰ-3	8.15	0.12	289.1	359.5	362.4	0.798	0.992

The crack initiation stress ratio (crack initiation stress/peak stress) is about 68%, and the crack damage stress ratio (crack damage stress/peak stress) is 94%. The crack damage stress is approximate to the peak stress, indicating that the internal cracks in the sample will rapidly propagate and split the sample when the peak stress is exceeded. Due to the concentrated and violent energy release, the sample will rupture instantaneously, and a

significant stress drop is observed in the stress–strain curve.

3.2 Brittleness index

The pre-peak brittleness index B_{i1} is used to describe the brittleness characteristics of granite failure[22], which can be calculated by

$$B_{i1}=\frac{\sigma_c-\sigma_{ci}}{\dfrac{\sigma_c}{\dfrac{\varepsilon_c-\varepsilon_i}{\varepsilon_c}}} \tag{3}$$

where ε_i is the axial strain corresponding to the crack initiation stress; and ε_c is the peak strain.

The brittleness index B_{i1} of each sample can be calculated by Eq 3, as shown in Table 2.

Table 2 Brittleness index B_i

Brittleness index	I-1	I-2	I-3
B_{i1}	0.82	0.84	0.99

3.3 Failure characteristics

Figure 6 shows the failure mode of a granite sample under a true triaxial loading path, in which the solid black line represents shear cracks, and the black dashed line represents tensile cracks. The mixed tensile-shear failure is observed on the failure surface of the sample. Many shear cracks and a few numbers of tensile cracks can be found on the surface of the sample. Along the directional plane σ_3, there are mainly tensile cracks formed by splitting failure and a small number of shear cracks formed by shearing failure. Because $\sigma_2 > \sigma_3$, the lateral deformation of the rock sample is along the σ_3 direction, and the development of internal cracks in the rock sample is induced during the loading process. Meanwhile, most of the cracks appear on the active surface of σ_2 and grow along the σ_2 direction. Then the crack splits the sample along the direction σ_2, which contributes to the formation of the main fracture surface that penetrates the entire sample.

4 Result analysis of true triaxial unloading tests for granite

4.1 Stress-strain curve

The true triaxial unloading failure test with an unloading rate of 0.3 mm/min is taken as an example for analysis in this study. The axial stress-strain curve and the crack volumetric strain-axial strain curve are plotted in Figs.7(a) and 7(b) respectively. In Fig.7, the stress-strain curve of the samples is divided into the initial compaction stage, the elastic deformation stage, the stable crack growth stage, and the unstable crack growth stage. After the unloading point *C*, the axial stress begins to decrease with the increase of the axial strain, which indicates that the granite sample loses its bearing capacity instantly and breaks down when the unloading starts.

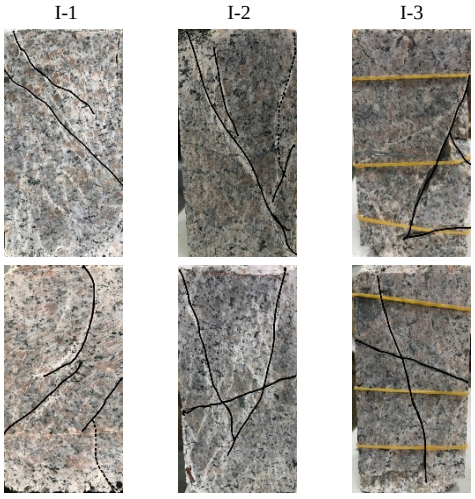

(a) Along the σ_2 direction

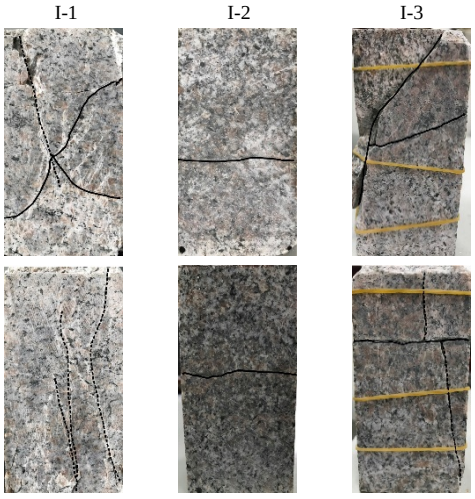

(b) Along the σ_3 direction

Fig. 6 Macroscopic failure characteristics of rock samples in true triaxial loading tests

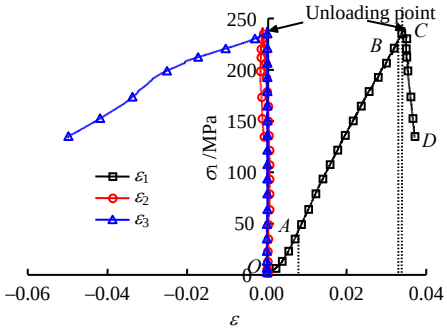

(a) Stress–strain curve

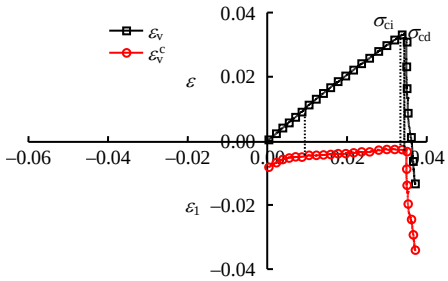

(b) Crack volumetric strain

Fig. 7 Stress–strain curves of true triaxial unloading tests

Figure 8 shows the relationship between the axial stress of granite and the principal strains in three directions under true triaxial unloading conditions. The axial stress-axial strain curves of granite under different unloading rates are consistent at the initial compaction stage of the test, and the curves are almost linear after the elastic deformation stage. In Fig.8(b), the changing trend of the maximum principal stress σ_1 as a function of the lateral strain ε_2 under different unloading rates is the same. In the compaction stage *OA*, the sample is compressed along the σ_2 direction, and the lateral strain ε_2 also increases slightly. The lateral strain ε_2 in the elastic deformation stage *AB* remains unchanged with the increase in σ_1. During the crack growth stage *BC*, the sample changes from volumetric compression to volumetric expansion along the σ_2 direction, and the lateral strain ε_2 begins to grow in the negative direction. In the unloading stage *DE*, a strong expansion along the σ_3 direction can be observed in the sample due to the decrease in the minimum principal stress σ_3. In order to keep the lateral stress σ_2 constant, the sample is slightly compressed along the σ_2 direction, and the lateral strain ε_2 can increase in the positive direction.

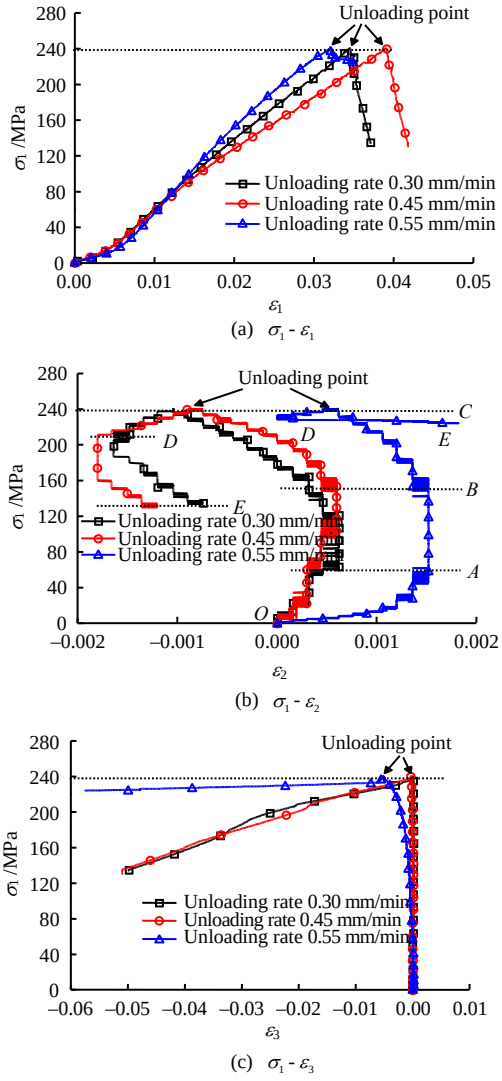

Fig. 8 Relationship between the axial stress of granite and the principal strains in three directions under true triaxial unloading conditions

According to Fig.8(c), the value of ε_3 during the loading stage remains almost unchanged. During the unloading stage, the lateral strain ε_3 increases significantly in the negative direction because the sample quickly ruptures and expands along the unloading direction.

4.2 Characteristic stress

As shown in Fig.8(b), the crack volumetric strain curve under the unloading path starts to increase rapidly at the unloading point, while the total volumetric strain curve drops rapidly after unloading. The characteristic stresses are calculated by Eqs.(1) and (2). The crack initiation stress and damage stress of the granite sample under the true triaxial unloading paths are 229.0 MPa and 240.4 MPa, respectively. The peak stress is the axial stress at the unloading point of 240.6 MPa. Meanwhile, the damage stress of the granite sample is close to the peak stress under the true triaxial unloading path, and the damage stress ratio is about 99.9%, which indicates that cracks are generated within the sample instantaneously after unloading σ_3, and penetrate the sample rapidly. Therefore, the rupture time of the sample is short, which exhibits significant brittleness.

4.3 Failure mode

Figure 9 shows the failure mode of a granite sample under the true triaxial unloading path, in which the solid black line represents shear cracks, and the black dashed line represents tensile cracks. The failure mode of the granite sample is also a combination of tensile and shear failure under true triaxial unloading conditions. Since only σ_3 is unloaded, the difference between σ_2 and σ_3 of the rock sample increases as the unloading continues. Then the lateral expansion of the rock sample occurs along the unloading direction. The macro-cracks are mainly generated on the active surface of σ_2 and propagate along the direction of σ_2. Two main fracture surfaces are formed and the rock sample is splitted into two parts eventually. Additionally, there are mainly shear cracks formed by shear failure, and a small number of tensile cracks formed by splitting failure on the surface along the σ_3 direction. Moreover, the deformation and failure of granite during unloading are more severe than that during loading, and the failure is accompanied with a loud noise.

4.4 Brittleness index

In the brittle failure process of rocks, cracks initiated and propagated as the external stress continues to increase. Then the fracture damage caused by further crack propagation occurs in this process. Therefore, it is of great significance to study the stress and strain change at the pre-peak crack growth stage for evaluating the rock brittleness. Although the brittleness index selected in Section 3.2 can better reflect the changes in the stress and strain in the crack growth stage, it is still not easy to calculate the crack initiation stress. Thus, the equation of brittleness index is modified in this section.

As mentioned above, the crack volumetric strain remains almost unchanged in the elastic stage. Then an inflection point can be observed on the crack volumetric strain curve. The crack volumetric strain increases, and

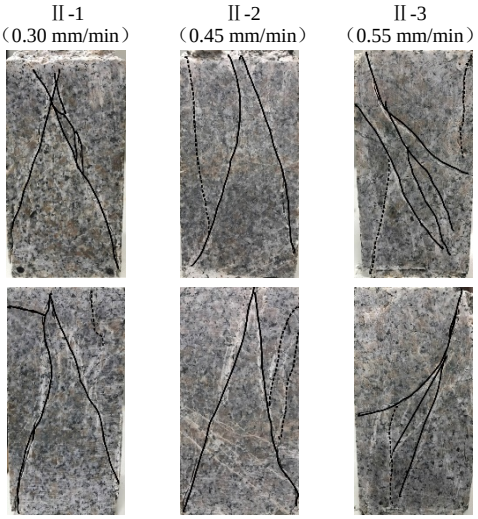

(a) Along the σ_2 direction

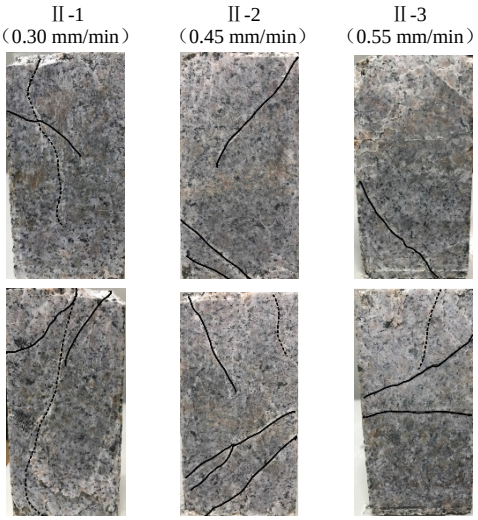

(b) Along the σ_3 direction

Fig. 9 Macroscopic failure characteristics of rocks under different unloading rates

the damage appears at this moment. When an inflection point of the volumetric strain appears, the volume of the rock sample changes from a compressed state to an expanded state, and the crack growth turns to be unstable. Therefore, in order to facilitate the calculation, the axial strain and damage stress corresponding to the inflection point of the volumetric strain curve are selected to calculate a new brittleness index as

$$B' = \frac{\dfrac{\sigma_{\mathrm{cd}} - \sigma_{\mathrm{c}}}{\sigma_{\mathrm{c}}}}{\dfrac{\varepsilon_{\mathrm{cd}} - \varepsilon_{\mathrm{c}}}{\varepsilon_{\mathrm{c}}}} \tag{4}$$

where $\varepsilon_{\mathrm{cd}}$ is the axial strain corresponding to damage stress.

From Eq (4), it is found that if the difference between the damage strain and the peak strain of the two types of rock samples is the same, the rock sample whose damage stress increases to the peak stress with a larger amplitude will be more brittle when damage occurs. If the difference between the initiation stress and the peak stress of the two rock samples is the same, the brittleness of the rock sample with a smaller strain increase will be stronger when damage happens.

Table 3 illustrates the brittleness index of each rock sample in true triaxial loading and unloading tests. It is found that the brittleness of granite is stronger under true triaxial unloading conditions, which is consistent with the test results. Therefore, this index can better evaluate the brittle state of rock.

Table 3 Brittleness index B'

Brittleness index	Loading test			Unloading test		
	Ⅰ-1	Ⅰ-2	Ⅰ-3	Ⅱ-1	Ⅱ-2	Ⅱ-3
B'	0.41	0.52	0.72	1.17	1.08	1.16

5 Energy analysis of true triaxial unloading tests for granite

5.1 Principle of the energy method

The axial energy–strain curve and the total energy–strain curve throughout tests can be obtained based on the results of the true triaxial loading and unloading tests. The axial energy absorbed by the rock sample is defined as the axial work applied by the testing machine on the rock sample as[14]

$$E_1 = \int \sigma_1 \mathrm{d}\varepsilon_1 = \sum_{i=0}^{n} \frac{1}{2}\left(\varepsilon_{1i+1} - \varepsilon_{1i}\right)\left(\sigma_{1i} + \sigma_{1i+1}\right) \tag{5}$$

where σ_1 and ε_1 are the axial stress and the axial strain, respectively; σ_{1i} and ε_{1i} are the axial stress and the axial strain corresponding to the calculation point of the stress-strain curve.

The total energy absorbed by the rock sample in the true triaxial stress state is[12]

$$U = E_1 + E_2 + E_3 \tag{6}$$

where

$$E_2 = \int \sigma_2 \mathrm{d}\varepsilon_2 = \sum_{i=0}^{n} \frac{1}{2}\left(\varepsilon_{2i+1} - \varepsilon_{2i}\right)\left(\sigma_{2i} + \sigma_{2i+1}\right) \tag{7}$$

$$E_3 = \int \sigma_3 \mathrm{d}\varepsilon_3 = \sum_{i=0}^{n} \frac{1}{2}\left(\varepsilon_{3i+1} - \varepsilon_{3i}\right)\left(\sigma_{3i} + \sigma_{3i+1}\right) \tag{8}$$

where σ_{2i}, ε_{2i} and σ_{3i}, ε_{3i} are two lateral stresses and lateral strains corresponding to two calculation points.

According to the energy properties of rock deformation, the total absorbed energy of the rock sample is divided into elastic strain E_{e} and dissipated energy E_{d},

$$U = E_{\mathrm{e}} + E_{\mathrm{d}} \tag{9}$$

The equation for calculating the elastic strain energy in true triaxial tests is

$$E_{\mathrm{e}} = \frac{1}{2E}\left[\sigma_1^2 + \sigma_2^2 + \sigma_3^2 - 2\mu\left(\sigma_1\sigma_2 + \sigma_1\sigma_3 + \sigma_2\sigma_3\right)\right] \tag{10}$$

where E is the elastic modulus of the rock; μ is the Poisson's ratio; E and μ are computed from the elastic deformation stage in the true triaxial loading test and the energy unit is MJ/m^3.

5.2 Energy evolution in loading tests

The energy evolution curves during the true triaxial loading test are shown in Fig.10. At the initial compaction stage *OA*, the total energy grows slowly, and the energy absorbed by the rock sample is used for the closure of the initial crack, friction and slippage. In the linear elastic stage *AB*, the original internal micro-cracks are compacted, and the stress concentration at the crack tip leads to the initiation and propagation of micro-cracks. The dissipated energy increases slowly in this stage, and the total energy curve is not entirely straight. In addition, the energy absorbed by the rock sample is mainly stored in the form of elastic strain energy. During the stable crack growth stage *BC*, energy is required for the internal crack penetration, the generation and expansion of macro-cracks, and the proportion of dissipated energy in the energy distribution also increases. Moreover, both the internal crack growth rate of the rock sample and the dissipation energy increase in the unstable crack growth stage *CD*. Due to the penetration of the macro-cracks, the sample expands in the direction of the minimum principal stress at the post-peak failure stage *DE*. In addition, the elastic strain energy is released at this stage, and the dissipated energy also increases significantly.

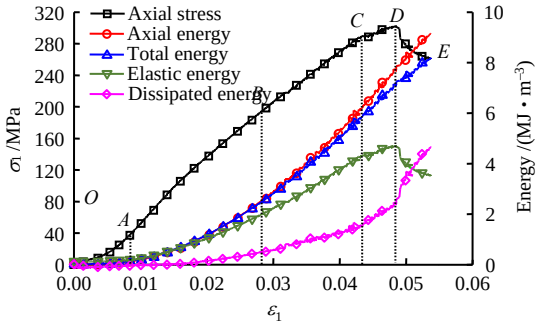

Fig. 10 Energy curves of true triaxial loading tests

5.3 Energy evolution in unloading tests

The energy evolution curves during the true triaxial unloading test at different unloading rates are shown in Fig.11. The changes in different energy curves are consistent with the loading test during the loading stage. In the unloading stage, macroscopic failure is observed in the sample at the moment of unloading and the failure expands rapidly along the unloading direction. Because huge energy is required for the macro-crack penetration and the sample expansion along the direction of the minimum principal stress, the dissipated energy increases rapidly, and its proportion of energy distribution exceeds the elastic strain energy, which becomes the dominant energy consumption.

By comparing the energy curves under three unloading rates, it is found that the effect of the unloading rate in the unloading test on the energy evolution is not evident. This is because unloading rates selected in the tests are fast and close to each other.

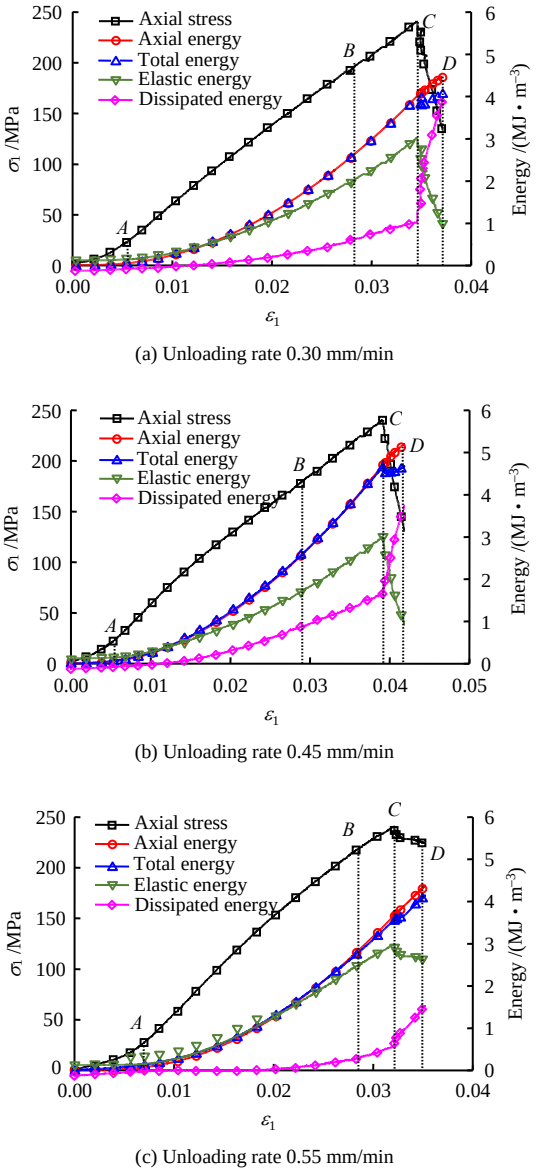

(a) Unloading rate 0.30 mm/min

(b) Unloading rate 0.45 mm/min

(c) Unloading rate 0.55 mm/min

Fig. 11 Energy curves of true triaxial unloading tests

5.4 Energy comparison in loading and unloading tests

The curves of dissipated energy–axial strain are shown in Fig.12. At the early stage of the test, the dissipated energy is almost 0. With an increase in the axial deformation, cracks are generated within the sample and the dissipated energy increases with a gradually increasing rate. When the axial stress reaches the peak stress in the loading test (the unloading point is achieved), the dissipated energy evidently increases, and an inflection point is observed. Moreover, the growth rate further increases. After that, the dissipated energy increases steadily, and the growth rate slows down. In the loading test, the dissipated energy is obviously greater than that in the unloading test when the sample is damaged. However, the increase of the dissipated energy in the unloading test is larger than that in the loading test when the sample is damaged. Therefore, more energy is consumed for the sample under the loading path to cause failure, and more elastic strain energy can be released under the unloading path,

which is more dangerous than the loading path.

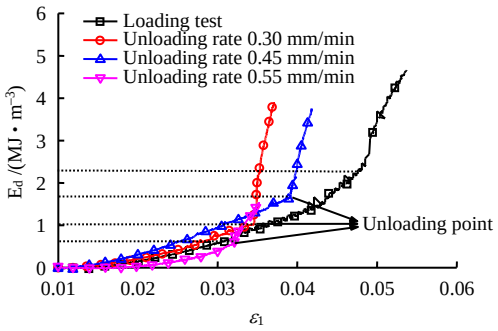

Fig. 12 Comparison of energy–strain curves in true triaxial loading and unloading tests

6 Conclusions

(1) Under the two true triaxial stress paths of loading and unloading, the failure mode of granite is a kind of mixed tensile-shear failure. The macro-cracks of the rock sample mainly grow and penetrate the sample along the σ_2 direction, and the rock sample expands evidently along the σ_3 direction.

(2) A novel brittleness index is proposed using the damage stress and axial strain corresponding to the inflection point of the volumetric strain curve. It can be judged based on the pre-peak curve, which can better evaluate the rock brittleness. Additionally, it is found that the brittleness of granite under the unloading path is stronger than that in loading path.

(3) The total energy curve has undergone an evolution process of slow increase, rapid increase, and steady increase under the true triaxial loading stress path. In the post-peak failure stage, the elastic strain energy is released rapidly, and the proportion of dissipated energy in energy distribution also increases dramatically.

(4) Under the true triaxial unloading stress path, the dissipated energy increases rapidly at the moment of unloading. Compared to the loading path, less energy is required for the sample under the unloading path to cause macroscopic failure, indicating that the unloading path is more dangerous.

References

[1] HE Man-chao, MIAO Jin-li, LI De-jian, et al. Experimental study on rockbust processes of granite specimen at great depth[J]. Chinese Journal of Rock Mechanics and Engineering, 2007, 26(5): 865–876.

[2] FENG Xia-ting, XIAO Ya-xun, FENG Guang-liang, et al. Study on the development process of rockbursts[J]. Chinese Journal of Rock Mechanics and Engineering, 2019, 38(4): 649–673.

[3] HE M C, ZHAO F, CAI M, et al. A novel experimental technique to simulate pillar burst in laboratory[J]. International Journal of Rock Mechanics and Mining Sciences, 2015, 48(5): 1833–1848.

[4] CHEN Jing-tao, FENG Xia-ting. True triaxial experimental study on rock with high geostress[J]. Chinese Journal of Sciences Mechanics and Engineering, 2006, 25(8): 1537–1543.

[5] FENG G L, FENG X T, CHEN B R, et al. Effects of structural planes on themicroseismicity associated with rockburst development processes in deep tunnels of the Jinping-II Hydropower Station, China[J]. Tunnelling and Underground Space Technology, 2019, 84: 273–280.

[6] SU Guo-shao, YAN Si-zhou, YAN Zhao-fu, et al. Evolution characteristics of acoustic emission in rockburst process under true-triaxial loading conditions[J]. Rock and Soil Mechanics, 2019, 40(5): 1673–1682.

[7] LI X B, FENG F, LI D Y, et al. Failure characteristics of granite influenced by sample height-to-width ratios and intermediate principal stress under true-triaxial unloading conditions[J]. Rock Mechanics and Rock Engineering, 2018, 51: 1321–1345.

[8] RONG Hao-yu, LI Gui-chen, ZHAO Guang-ming, et al. True triaxial test study on mechanical properties of deep rock mass in different stress paths[J]. Journal of China Coal Society, 2020, 45(9): 3140–3149.

[9] KONG R, TUNCAY ERGÜN, ULUSAY RESAT, et al. An experimental investigation on stress-induced cracking mechanisms of a volcanic rock[J]. Engineering Geology, 2021, 280: 1–11.

[10] ZHANG Jun-wen, FAN Wen-bing, SONG Zhi-xiang, et al. Mechanical characteristics of deep under different true triaxial stress path[J]. Journal of China University of Mining & Technology, 2021, 50(1): 106–114.

[11] XIE He-ping, JU Yang, LI Li-yun, et al. Energy mechanism of deformation and failure of rock masses[J]. Chinese Journal of Rock Mechanics and Engineering, 2008, 27(9): 1729–1740.

[12] XIE He-ping, JU Yang, LI Li-yun. Criteria for strength and structural failure of rocks based on energy dissipation and energy release principles[J]. Chinese Journal of Rock Mechanics and Engineering, 2005, 24(17): 3003–3010.

[13] ZHANG Zhi-zhen, GAO Feng. Experimental research on energy evolution of red sandstone samples under uniaxial compression[J]. Chinese Journal of Rock Mechanics and Engineering, 2012, 31(5): 953–962.

[14] SU Guo-shao, JIANG Jian-qing, FENG Xia-ting, et al. Experimental study of ejection process in rockburst[J]. Chinese Journal of Rock Mechanics and Engineering,

2016, 35(10): 1990–1999.

[15] SU G S, JIANG J Q, ZHAI S B, et al. Influence of tunnel axis stress on strainburst: an experimental study[J]. International Journal of Rock Mechanics and Mining Sciences, 2017, 50(6): 1551–1567.

[16] CONG Yu, WANG Zai-quan, ZHENG Ying-ren, et al. Energy evolution principle of fracture propagation of marble with different unloading stress paths[J]. Journal of Central South University (Science and Technology). 2016, 49(7): 3140–3147.

[17] ZHANG Li-ming, GAO Su, WANG Zai-quan, et al. Analysis of marble failure energy evolution under loading and unloading conditions[J]. Chinese Journal of Rock Mechanics and Engineering, 2013, 32(8): 1572–1578.

[18] ZHANG L M, CONG Y, MENG F Z, et al. Energy evolution analysis and failure criteria for rock under different stress paths[J]. Acta Geotechnia, 2021, 16(2): 569–580.

[19] ZHANG L M, GAO S, WANG Z Q, et al. Analysis on deformation characteristics and energy dissipation of marble under different unloading rates[J]. Technical Gazette, 2014, 21: 987–999.

[20] MA Xiao, MA Dong-dong, HU Da-wei, et al. A real-time high-temperature true triaxial test system and its application[J]. Chinese Journal of Rock Mechanics and Engineering, 2019, 38(8): 1605–1614.

[21] MARTIN C. D. The strength of massive Lac du Bonnet granite around underground openings[D]. Winnipeg: University of Manitoba, 1993.

[22] CHEN Guo-qing, ZHAO Cong, WEI Tao, et al. Evaluation method of brittle characteristics of rock based on full stress-strain curve and crack initiation stress[J]. Chinese Journal of Rock Mechanics and Engineering, 2018, 37(1): 51–59.